

## Photodissociation dynamics of $\text{IBr}^-(\text{CO}_2)_n$ , $n < 15$

Todd Sanford, Sang-Yun Han, Matthew A. Thompson, Robert Parson,  
and W. Carl Lineberger

*JILA and Department of Chemistry and Biochemistry, University of Colorado, Boulder, Colorado 80309*

(Received 29 September 2004; accepted 2 November 2004; published online 18 January 2005)

We report the ionic photoproducts produced following photoexcitation of mass selected  $\text{IBr}^-(\text{CO}_2)_n$ ,  $n=0-14$ , cluster ions at 790 and 355 nm. These wavelengths provide single state excitation to two dissociative states, corresponding to the  $A' \ ^2\Pi_{1/2}$  and  $B \ 2 \ ^2\Sigma_{1/2}^+$  states of the  $\text{IBr}^-$  chromophore. Excitation of these states in  $\text{IBr}^-$  leads to production of  $\text{I}^- + \text{Br}$  and  $\text{Br}^- + \text{I}^*$ , respectively. Potential energy curves for the six lowest electronic states of  $\text{IBr}^-$  are calculated, together with structures for  $\text{IBr}^-(\text{CO}_2)_n$ ,  $n=1-14$ . Translational energy release measurements on photodissociated  $\text{IBr}^-$  determine the  $\text{I}-\text{Br}^-$  bond strength to be  $1.10 \pm 0.04$  eV; related measurements characterize the  $A' \ ^2\Pi_{1/2} \leftarrow X \ ^2\Sigma_{1/2}^+$  absorption band. Photodissociation product distributions are measured as a function of cluster size following excitation to the  $A' \ ^2\Pi_{1/2}$  and  $B \ 2 \ ^2\Sigma_{1/2}^+$  states. The solvent is shown to drive processes such as spin-orbit relaxation, charge transfer, recombination, and vibrational relaxation on the ground electronic state. Following excitation to the  $A' \ ^2\Pi_{1/2}$  electronic state,  $\text{IBr}^-(\text{CO}_2)_n$  exhibits size-dependent cage fractions remarkably similar to those observed for  $\text{I}_2^-(\text{CO}_2)_n$ . In contrast, excitation to the  $B \ 2 \ ^2\Sigma_{1/2}^+$  state shows extensive trapping in excited states that dominates the recombination behavior for all cluster sizes we investigated. Finally, a pump-probe experiment on  $\text{IBr}^-(\text{CO}_2)_8$  determines the time required for recombination on the ground state following excitation to the  $A'$  state. While the photofragmentation experiments establish 100% recombination in the ground electronic state for this and larger  $\text{IBr}^-$  cluster ions, the time required for recombination is found to be  $\sim 5$  ns, some three orders of magnitude longer than observed for the analogous  $\text{I}_2^-$  cluster ion. Comparisons are made with similar experiments carried out on  $\text{I}_2^-(\text{CO}_2)_n$  and  $\text{ICl}^-(\text{CO}_2)_n$  cluster ions. © 2005 American Institute of Physics. [DOI: 10.1063/1.1839178]

### I. INTRODUCTION

Chemists have long known that the course of a chemical reaction is profoundly influenced by the local environment of the reacting species. Rates, mechanisms, and even the final products of solution-phase reactions often differ drastically from those of their gas-phase counterparts. The mechanisms that give rise to this sensitive dependence can be grouped into two classes. At one level, the solvent acts as a medium for energy exchange, helping to promote reactants over an activation barrier and to stabilize the nascent products by dissipating the heat produced. At a deeper level, the solvent perturbs the potential energy surfaces that govern the reaction, by (for example) changing the relative energies of alternative product channels, raising or lowering barriers, and inducing nonadiabatic electronic transitions. Solvent effects of the second class are particularly important in reactions that involve a substantial redistribution of electronic charge, since the relatively localized charge distributions of stable molecules interact differently with the solvent than the more extended charge distributions of species near their transition states.

Solvent effects of both types can be clearly seen in a simple prototype reaction, the environment-induced recombination or “caging” of a photodissociated diatomic molecule. Since it was first identified<sup>1-3</sup> in the 1930s, this process has been widely studied in liquid solution,<sup>4-12</sup> high-

pressure gases,<sup>13-18</sup> solid matrices,<sup>19-23</sup> and most recently in gas-phase molecular clusters. Clusters provide an appealing medium in which to study solvation, because they offer well-defined microscopic environments that retain many of the characteristics and properties of their condensed phase counterparts.<sup>24-27</sup> This is especially true for ionic clusters, since ions of a desired mass can be selected by mass spectrometry; thus allowing for some degree of control over the configuration of the local solvent environment. In such experiments, one does not attempt to simply reproduce the condensed phase behavior; instead, the gas-phase clusters provide one with a well-characterized environment in which important condensed phase interactions can be isolated for detailed study.

Much of the recent experimental and theoretical work on the cage effect has focussed on dihalide ions such as  $\text{I}_2^-$  and  $\text{ICl}^-$ . On the experimental side, these molecular anions are relatively easy to produce and possess low-lying dissociative electronic states, allowing for photolysis using visible or near-UV radiation. On the theoretical side, they are small enough to allow for high-level *ab initio* calculations of excited as well as ground state potential curves. They also have intrinsic theoretical interest, because the interaction between the solute charge and the polarizable solvent competes with the chemical bonding interactions within the solute, leading to extensive solvent perturbations of the solute electronic structure. For example, the dissociation energy<sup>28,29</sup> of  $\text{I}_2^-$  is

1.01 eV and that of  $\text{ICl}^-$  is only slightly higher<sup>30</sup> at 1.07 eV, while the typical first solvation shell binding energy of a  $\text{CO}_2$  molecule to these anions<sup>31</sup> is  $\sim 0.2$  eV, so that in a cluster of four or more  $\text{CO}_2$  molecules the total solvation energy is comparable to the solute bond strength.

Prior dihalide photofragmentation studies focussed on  $\text{ICl}^-$ ,  $\text{Br}_2^-$ , and  $\text{I}_2^-$  solutes in mass selected clusters of Ar,  $\text{CO}_2$ , and OCS. Photofragmentation studies of  $\text{ICl}^-$  embedded<sup>30</sup> in  $\text{CO}_2$  and  $\text{I}_2^-$  in OCS and  $\text{CO}_2$  clusters<sup>31–34</sup> find remarkably different photofragment product distributions following excitation to similar dissociative electronic states. These results show increasing recombination with increasing cluster size in solvated  $\text{I}_2^-$  and the charge-transfer, dissociated product  $\text{Cl}^-$  dominating at larger cluster sizes in the  $\text{ICl}^-(\text{CO}_2)_n$  clusters. Pump-probe experiments were carried out on solvated  $\text{I}_2^-$  to determine recombination and vibrational relaxation times after excitation to various excited electronic states.<sup>31–33,35–40</sup> A relevant conclusion drawn collectively from these time-resolved studies is that, whenever 100% recombination occurs, the time required for recombination is of order 20 ps. Until now, there have been no time-resolved studies in the gas phase on dihalide anions other than  $\text{I}_2^-$ .

The  $\text{IBr}^-$  anion was chosen for this study in part because of the size difference between Br and I atoms. This size difference ensures that initial solvation takes place about the smaller, Br end of  $\text{IBr}^-$ , a supposition that we confirm with structure calculations. The asymmetric anion also affords unequivocal identification of the electronic states accessed during photoexcitation, identification that was ambiguous in the case of  $\text{I}_2^-$ .

The  $\text{IBr}^-$  photoabsorption spectrum and photofragment products are determined by cross section measurements across the  $A' \ ^2\Pi_{1/2} \leftarrow X \ ^2\Sigma_{1/2}^+$  absorption band. Photofragment translational energy release measurements are carried out to determine the transition dipole moment orientation and the bond strength of  $\text{IBr}^-$ . The photofragmentation branching ratios of  $\text{IBr}^-(\text{CO}_2)_n$  clusters ( $n=0–14$ ) are obtained at a series of wavelengths corresponding to excitation to both the  $A' \ ^2\Pi_{1/2}$  and  $B \ ^2\Sigma_{1/2}^+$  electronic states. The branching ratios provide the data needed to carry out a pump-probe experiment to determine the time scale for recombination of  $\text{IBr}^-(\text{CO}_2)_8$  on the ground  $^2\Sigma_{1/2}^+$  state, following excitation to the  $A'$  state.

The experimental results for solvated  $\text{IBr}^-$  are then compared with the results of similar experiments on  $\text{ICl}^-(\text{CO}_2)_n$  and  $\text{I}_2^-(\text{CO}_2)_n$  cluster ions. These comparative studies are used to present an overall picture of the role of various dihalide solutes in determining the solvation dynamics. The calculated potentials and cluster structures provide important guidance and insight throughout the process.

## II. THEORETICAL

The theoretical methods used in this investigation have been described in detail elsewhere.<sup>41,42</sup> We give only a brief summary here, focusing on those aspects of the calculations that differ materially from the earlier work; a more complete description will be published elsewhere.

The  $\text{IBr}^-$  potential energy curves, together with associated electronic properties such as charge distributions and transition moments, are obtained from high-level *ab initio* calculations using the MOLPRO 2002.6 package.<sup>43</sup> These calculations use the internally contracted multireference configuration interaction methods developed by Knowles and Werner<sup>44–46</sup> and the energy-consistent effective core potential (ECP) of the Stuttgart-Bonn group,<sup>47</sup> specifically, the large-core MDF ECPs that are based upon multiconfiguration Dirac–Hartree–Fock calculations of the neutral atom. The basis sets are an augmented form,  $(7s7p3d2f)/[5s5p3d2f]$ , of the stock  $(6s6p)/[4s4p]$  basis sets included with the ECPnMDF ECPs.<sup>47,48</sup> In contrast to our earlier calculations<sup>49</sup> on  $\text{I}_2^-$  and  $\text{ICl}^-$ , which relied on a semiempirical treatment of spin-orbit coupling, the present calculations include a spin-orbit ECP and a core polarization potential, which models the charge-induced dipole interaction of the core. The reference orbitals and configurations are obtained from state-averaged complete active-space self-consistent field calculations<sup>50,51</sup> that consisted of 15 electrons in the lowest two  $\Sigma$ ,  $\Pi_x$ , and  $\Pi_y$  states that arise from the  $^2P$  state of the neutral and the  $^1S$  state of the ion. A spin-orbit (SO) calculation of all six states is then performed using SO-ECPs.<sup>52</sup> This calculation is carried out at 42 bond lengths ranging from 4.5 to  $100a_0$ .

The minimum energy structures for the  $\text{IBr}^-(\text{CO}_2)_n$  clusters ( $n=0–14$ ) are generated using the effective Hamiltonian model developed by Maslen, Faeder, and Parson<sup>41,53–56</sup> previously employed in characterization of the structure of  $\text{I}_2^-(\text{CO}_2)_n$  cluster ions.<sup>57</sup> In this model, the charge distribution on the  $\text{IBr}^-$  anion is obtained from a distributed multipole analysis of the *ab initio* wavefunctions. The Mulliken charge distribution is calculated to be  $-0.44$  on I and  $-0.56$  on Br in unsolvated  $\text{IBr}^-$ . The charge distribution changes to  $-0.34$  on I and  $-0.66$  on Br in  $\text{IBr}^-(\text{CO}_2)_8$  where the asymmetric solvation is quite large. The inclusion of distributed transition moments—elements of the density matrix that are off diagonal with respect to the electronic states of the isolated solute—allows for polarization of the solute charge cloud by the solvent. The charge distribution and polarizability of the solvent molecules are taken from a model used for condensed phase simulations. The long-range electrostatic and induction interactions between solute and solvent are calculated explicitly from the charges and polarizabilities, while the short-range interactions are treated empirically, using atom-atom Lennard-Jones potentials with parameters taken from a wide variety of experiments.<sup>41</sup> In subsequent molecular dynamics calculations, forces are calculated from analytic gradients of the potentials.

In order to calculate equilibrium structures, for each cluster size 201 configurations are obtained by sampling a single 1 ns molecular dynamics trajectory having an average temperature of 80 K corresponding to the estimated experimental temperature. These configurations are then quenched to their lowest minima by means of an algorithm based upon Newton–Raphson optimization.<sup>58</sup> The geometries of these optimized cluster ions are available through EPAPS.<sup>59</sup>

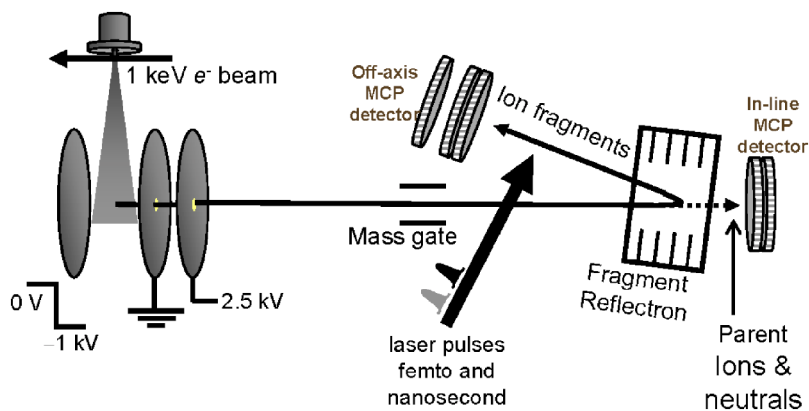


FIG. 1. Schematic diagram of the cluster ion source and tandem-time-of-flight mass spectrometers.

### III. EXPERIMENT

#### A. Overview

A schematic diagram of the cluster ion source, the tandem-time-of-flight mass spectrometer, and associated ion detectors is shown in Fig. 1. The  $\text{IBr}^-(\text{CO}_2)_n$  clusters are formed in a pulsed supersonic expansion containing IBr, Ar, and  $\text{CO}_2$ . The  $\text{IBr}^-$  ions are produced by low energy electron attachment to IBr in this expansion.<sup>27</sup> The anionic clusters are injected into a Wiley–McLaren time-of-flight mass spectrometer where the ions are mass selected and intersect a pulsed laser beam at the spatial focus of the time-of-flight mass spectrometer. The ionic photofragments are then mass analyzed by a secondary reflectron-type mass spectrometer and detected by a microchannel plate particle detector. A representative mass spectrum of the  $\text{IBr}^-(\text{CO}_2)_n$  clusters is shown in Fig. 2.

#### B. Ionic cluster production and photofragment mass analysis

The cluster ion source and tandem time-of-flight (TOF) mass spectrometer have been described in detail elsewhere.<sup>30,33</sup> The  $\text{IBr}^-(\text{CO}_2)_n$  clusters are produced by condensation of  $\text{CO}_2$  around the  $\text{IBr}^-$  charge centers created by attachment of slow secondary electrons produced by electron impact ionization of the pulsed supersonic expansion.<sup>27</sup>

The neutral expansion is produced by passing 2–3 atm of  $\text{CO}_2$  over a reservoir of solid IBr (Aldrich, 98% purity) through the 0.8 mm diameter nozzle of a supersonic expansion valve (General Valve Series 9) pulsed at 80 Hz. The reservoir and stainless steel lines between the reservoir and valve are typically heated to 50–60 °C. The electron impact ionization is produced by a 1 keV electron beam from an electron gun intersecting the expansion at the throat of the nozzle.<sup>27</sup> When arranged for collinear excitation,<sup>60</sup> a small ring magnet is attached to the valve faceplate to direct the electron beam into the expansion orifice. The cluster ions are estimated to have a temperature of around 40–50 K, based on RRKM calculations and analysis of evaporation patterns.<sup>61,62</sup> A new faceplate, based on the work of Even and Jortner,<sup>63,64</sup> was employed for the expansion valve, and it should afford better cooling of the cluster ions. A passivation time with IBr vapor of the gas lines and pulsed valve of about a week is required before  $\text{IBr}^-$  appears.

After a drift time of  $\sim 1$  ms, the negative ions are extracted into a differentially pumped Wiley–McLaren TOF mass spectrometer by a pulsed electric field ( $\sim 750$  V). The ions then enter an acceleration and ion optics stack where they are accelerated to 3 keV; horizontal and vertical deflectors and an einzel lens provide steering and focus the ion beam at the Wiley–McLaren spatial focus of the time of flight. At this point, the ion packet is intercepted with a softly

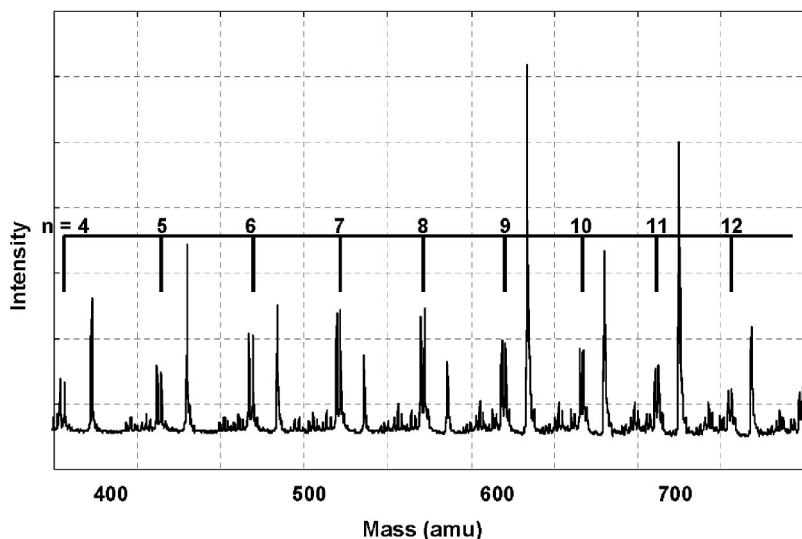


FIG. 2. Time-of-flight mass spectrum of the midsized  $\text{IBr}^-(\text{CO}_2)_n$  cluster ions, where  $n$  indicates the number of  $\text{CO}_2$  attached to  $\text{IBr}^-$ . The other prominent peaks are  $(\text{CO}_2)_n^-$  cluster ions.

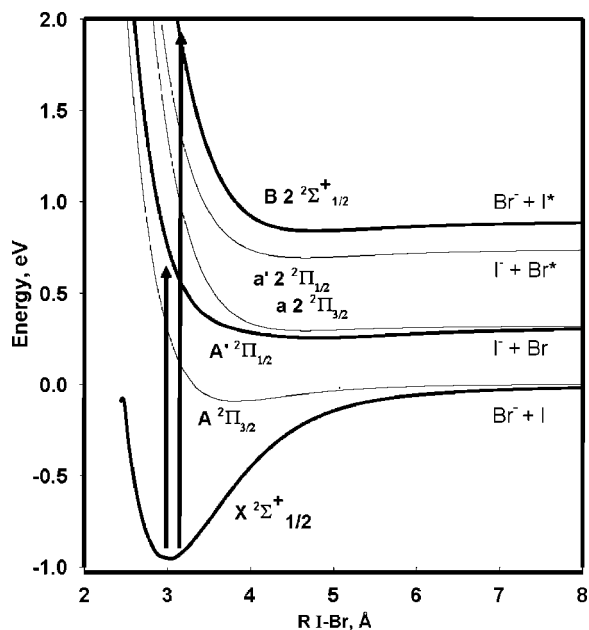


FIG. 3. Calculated potential energy curves for the lowest six electronic states of  $\text{IBr}^-$ . Arrows indicate the studied transitions to the  $A'$  and  $B$  states.

focused, pulsed laser beam. After the laser interaction region, there is a secondary TOF reflectron mass spectrometer that focuses the ionic photoproducts onto an off axis microchannel plate detector. An inline microchannel plate detector is also present to monitor the parent ions and to detect neutral products formed during photolysis.

### C. Laser systems

The nanosecond pulses used for the photodissociation cross sections and photofragmentation branching ratios were generated by using a Coherent Infinity Nd:yttrium aluminum garnet (YAG) pumped optical parametric oscillator, tunable from 210 to 2000 nm, with pulse energies of a few hundred microjoules to a few millijoules. The laser is operated at 80 Hz to match the repetition rate of the pulsed valve. The femtosecond pulses for the time-resolved experiments (790 nm, 3 mJ, 180 fs, 400 Hz) are generated by a Coherent Mira Ti:sapphire oscillator in combination with a Quantronix Titan stretcher/compressor and regenerative/multipass Ti:sapphire amplifiers pumped by a Quantronix Nd:YLF laser. The 400 Hz laser repetition rate is reduced to 80 Hz to match the maximum repetition rate of the pulsed valve. The 790 nm fundamental pulse is split into two identical parts (pump and probe), with the probe pulse being sent either through a variable delay stage for short pump-probe delays or a longer fixed-length optical path for nanosecond delays. Computer-controlled shutters are placed in each path for background measurements. Details of the laser system and data acquisition procedures have been presented elsewhere.<sup>33,35</sup>

## IV. RESULTS

We first characterize the spectroscopic properties of  $\text{IBr}^-$ . The calculated electronic potentials for the six lowest lying states of  $\text{IBr}^-$  are shown in Fig. 3. The electronic

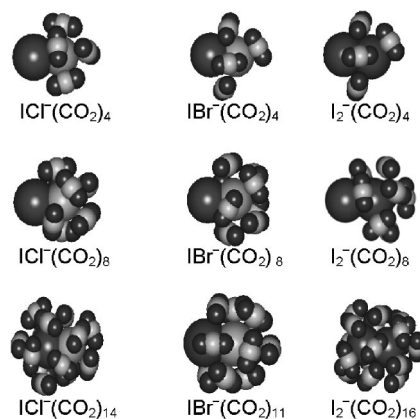


FIG. 4. Representative cluster structures calculated for  $\text{ICl}^-$ ,  $\text{IBr}^-$ , and  $\text{I}_2^-$  with various numbers of  $\text{CO}_2$  solvent molecules. The smaller halogen is always on the right side. Molecule coordinates for  $\text{IBr}^-$  clusters with 14 or fewer solvents are available through EPAPS (Ref. 59).

state(s) excited at various wavelengths are identified experimentally by both the direction of the transition moment and the identity of the ionic dissociation products. For the  $A' 2^2\Pi_{1/2} \leftarrow X 2^2\Sigma_{1/2}^+$  absorption band, careful measurements are also made of the shape, magnitude, and location of this band. The energy required to dissociate  $\text{IBr}^-$  to  $\text{I-Br}^-$  is obtained through measurements of the translational energy release following excitation to both the  $A' 2^2\Pi_{1/2}$  and  $B 2^2\Sigma_{1/2}^+$  states. The configuration of the first few solvent molecules about  $\text{IBr}^-$  reflects the stronger binding that comes from attachment to the smaller Br moiety. Representative structures of the  $\text{IBr}^-(\text{CO}_2)_n$  cluster ions calculated as described in Sec. II are shown in Fig. 4. The photofragmentation spectra of  $\text{IBr}^-(\text{CO}_2)_n$ ,  $n=0-15$ , cluster ions upon excitation to two electronic states ( $A' 2^2\Pi_{1/2}$  and  $B 2^2\Sigma_{1/2}^+$ ) of  $\text{IBr}^-$  are presented to illustrate the effects of the solvent. Finally, we report preliminary results of a pump-probe study to determine the time scale for recombination and vibrational relaxation on the ground state following excitation of  $\text{IBr}^-(\text{CO}_2)_8$  to the  $A' 2^2\Pi_{1/2}$  state.

### A. Spectroscopic characterization of $\text{IBr}^-$

The calculated potential energy curves for  $\text{IBr}^-$  are shown in Fig. 3. As with  $\text{I}_2^-$ , there are six valence states corresponding to a vacancy in each of the valence orbitals. While  $\text{I}_2^-$  has only two distinct dissociation limits, the heteronuclear  $\text{IBr}^-$  has four distinct dissociation limits. The two dissociative states with neutral iodine as a product are separated by the 0.94 eV iodine spin-orbit splitting.<sup>65</sup> The corresponding neutral bromine product curves have an asymptotic energy separation of 0.457 eV, reflecting the bromine spin-orbit splitting.<sup>66</sup> The calculated potential energy curves show that the excited states have either very shallow wells or are dissociative. Translational energy-release spectroscopy at a series of wavelengths between 660 and 790 nm is used to determine  $D_0(\text{I-Br}^-)$  to be  $1.10 \pm 0.04$  eV, making the bond strength comparable to that of  $\text{I}_2^-$  and  $\text{ICl}^-$ . The calculated  $D_0(\text{I-Br}^-)$  is found to be 0.955 eV and the calculated equilibrium bond length is 3.05 Å. The calculated ground state vibrational frequency is  $115 \text{ cm}^{-1}$ , but is calculated at a

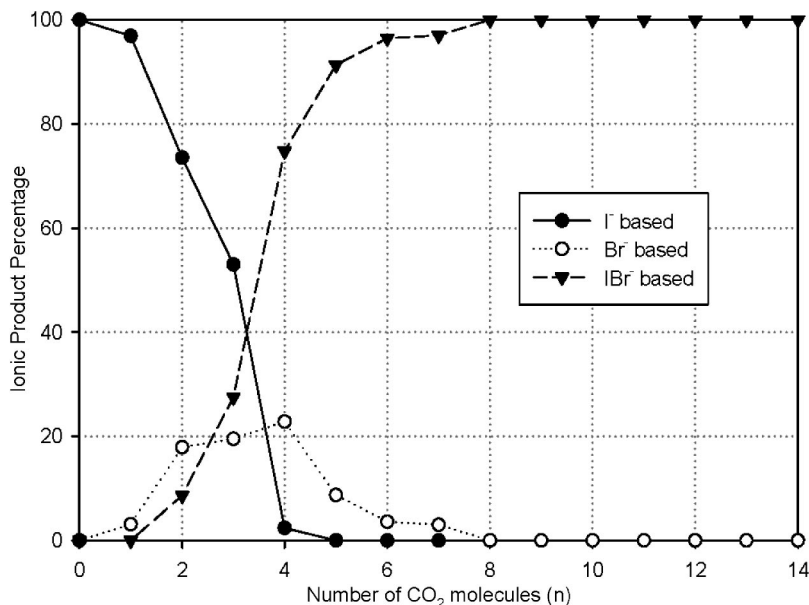


FIG. 5. Photofragmentation products of  $\text{IBr}^-(\text{CO}_2)_n$  cluster ions upon excitation to the  $A'$   $^2\Pi$  state with 790 nm photons and a kinetic energy release of 0.3 eV.

lower level of theory than that used for the calculation of the potential curves. The frequency is experimentally measured as  $136\text{ cm}^{-1}$  in solution<sup>67</sup> with no known gas-phase measurement. The presence of only  $\text{I}^-$  as a photoproduct at these wavelengths confirms that only one electronic state is excited, with dissociation taking place exclusively on the  $A'$  electronic state. Also, the transition to the  $A'$  state is observed to be a parallel transition, in accord<sup>31</sup> with the strong spin-orbit coupling in  $\text{IBr}^-$ .

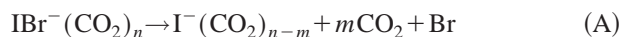
These measurements of the photodissociation cross section show the  $A' \leftarrow X$  absorption band to be a featureless, Gaussian-shaped band centered at  $\sim 740\text{ nm}$ , with a full-width half-maximum of  $\sim 50\text{ nm}$ . The absolute cross section is determined to be  $8.6 \times 10^{-18}\text{ cm}^2$  at  $760\text{ nm}$ , using  $\text{IBr}^-$  depletion to obtain the absolute cross section. This measurement gives an absolute  $\text{IBr}^-$  photoabsorption cross section of  $3 \times 10^{-18}\text{ cm}^2$  at  $790\text{ nm}$ , where the pump-probe studies are carried out.

Photoabsorption by  $\text{IBr}^-$  at  $355\text{ nm}$  produced only  $\text{Br}^-$  as a product ion, strongly suggesting this wavelength excites only the  $B\ 2^2\Sigma_{1/2}^+$  state. We have not carried out detailed photoabsorption measurements for the solvated anion,  $\text{IBr}^-(\text{CO}_2)_n$ . However previous work on  $\text{ICl}^-$  showed that there is very little change in the shape or location of these absorption bands upon addition of  $\text{CO}_2$  solvents.<sup>30</sup> It is assumed that  $\text{IBr}^-$  behaves in an analogous manner, with no significant change to the absorption cross sections upon solvation. With  $\text{IBr}^-$  now characterized, we can proceed to investigate the effect of  $\text{CO}_2$  solvation.

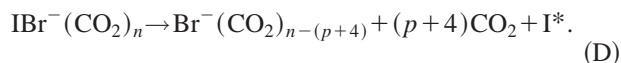
## B. Photofragmentation of $\text{IBr}^-(\text{CO}_2)_n$ upon excitation to the $A'$ $^2\Pi_{1/2}$ state

Photodissociation following excitation to the  $A'$   $^2\Pi_{1/2}$  state is investigated at a series of wavelengths ( $790$ ,  $760$ , and  $675\text{ nm}$ ) spanning the absorption band and providing energy releases of  $0.3$ ,  $0.35$ , and  $0.55\text{ eV}$ , respectively. Dissociation

in this state correlates to  $\text{I}^- + \text{Br}$  products. When  $\text{IBr}^-$  is solvated by  $\text{CO}_2$ , there are three distinguishable product channels:



Channel (A) corresponds to direct dissociation in the  $A'$  state, giving the expected  $\text{I}^-$ -based dissociation products. Channel (B) corresponds to cage recombination, reforming the dihalide anion on the ground electronic state after dissociation, with the number of solvents retained on the recombined products reflecting the extent of vibrational relaxation on the ground state. Channel (C) corresponds to a dissociative event following charge transfer from the initially formed  $\text{I}^-$  to the neutral  $\text{Br}$ . Both channels (B) and (C) represent processes that require solvent participation. For the larger clusters ( $n \geq \sim 4$ ), an additional channel producing spin-orbit excited iodine,  $\text{I}^*$ , is energetically accessible through the additional process



The  $A'$   $^2\Pi_{1/2}$  photofragmentation data provide no evidence for flux into this channel, and we do not discuss it further.

The photofragmentation products arising from excitation of  $\text{IBr}^-(\text{CO}_2)_n$  at  $790\text{ nm}$ , near the long wavelength end of the  $A'$  band, are presented in Fig. 5 as a function of cluster size. Excitation at this wavelength corresponds to an energy release of  $0.3\text{ eV}$  on the  $A'$  state. At this wavelength,  $\text{I}^-$  is the only ionic photoproduct when  $\text{IBr}^-$  is excited. The addition of a single solvent molecule is sufficient to allow a nonadiabatic transition to the ground electronic state, yielding the  $\text{Br}^-$  charge-transfer product ion. Addition of a second  $\text{CO}_2$  solvent molecule increases the yield of the  $\text{Br}^-$ -based charge-transfer products and the first recombined  $\text{IBr}^-$ -based

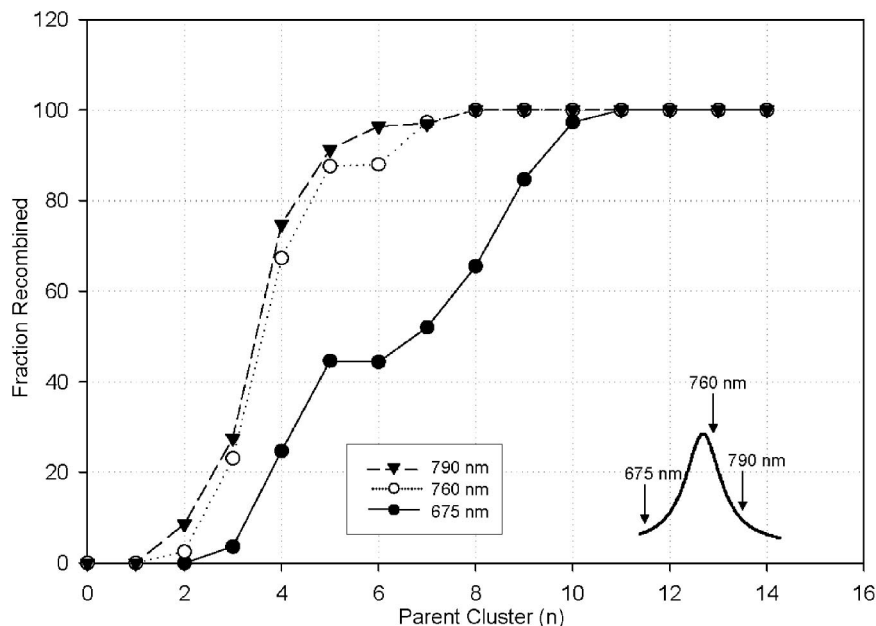


FIG. 6. Recombination efficiency across the  $A'$  absorption band in  $\text{IBr}^-(\text{CO}_2)_n$  cluster ions. The excitation wavelengths are 790, 760, and 675 nm corresponding to energy releases on  $A'$  of 0.30, 0.35, and 0.55 eV, respectively. The locations of the wavelengths on the  $A'$  band are also shown in the inset.

products on the ground electronic state appear. As the number of  $\text{CO}_2$  solvents is increased, the recombined products quickly dominate, and the “direct,”  $\text{I}^-$ -based dissociation products disappear. The charge-transfer  $\text{Br}^-$ -based products persist in small quantities up to  $n=7$ , after which the only products correspond to recombination in the ground electronic state. Although  $\text{Br}^-$ -based products are observed only for 1–7 solvent molecules, solvent driven charge transfer is clearly demonstrated to occur before recombination occurs.

Similar measurements are taken at 760 and 675 nm, spanning the  $A' \ ^2\Pi_{1/2}$  absorption band and providing 0.35 and 0.55 eV energy releases, respectively. While similar charge-transfer processes are again observed, Fig. 6 focuses on the recombination probability as a function of energy release and cluster size. The two wavelengths (760 and 790 nm) corresponding to nearly equal kinetic energy release show very similar recombination behavior, with the first recombined products seen at  $n=2$ , and 100% recombination attained by  $n=8$ . The 675 nm excitation provides a kinetic energy release  $\approx 0.2$  eV greater than that available at the other wavelengths. As this energy is approximately the binding energy of one solvent molecule, one might expect the 675 nm recombination curve in Fig. 6 to be shifted one solvent up from the other curves. While the onset of recombined products occurs one solvent molecule higher, the shapes are quite different, and the overall shift in the 5–11 solvent range is almost four solvent molecules. Simple energetic arguments cannot account for such behavior, and detailed simulations, similar to those previously reported<sup>41,68</sup> for  $\text{I}_2^-$ , will be needed for full understanding of the solvent effects.

### C. Photofragmentation of $\text{IBr}^-(\text{CO}_2)_n$ upon excitation to the $B \ 2 \ ^2\Sigma_{1/2}^+$ state

Photodissociation studies upon excitation to the  $B \ 2 \ ^2\Sigma_{1/2}^+$  state are carried out in an analogous manner to those described above for the  $A'$  state studies, with complete

characterization taking place at one wavelength (355 nm). Photoabsorption by  $\text{IBr}^-$  at 355 nm excites only the  $B \ 2 \ ^2\Sigma_{1/2}^+$  state, with  $\text{Br}^-$  and  $\text{I}^*$  dissociation products and 1.75 eV energy release. With the addition of solvent molecules, five lower-energy dissociative channels become possibilities (Fig. 3), corresponding to  $\text{I}^- + \text{Br}^*$ ,  $\text{I}^- + \text{Br}$ , and  $\text{Br}^- + \text{I}$  products.

The photofragmentation product distribution for  $\text{IBr}^-(\text{CO}_2)_n$  ( $n=0-11$ ) following 355 nm excitation to the  $B \ 2 \ ^2\Sigma_{1/2}^+$  state is depicted in Fig. 7. With the addition of the first  $\text{CO}_2$  solvent molecule, the  $\text{I}^-$  charge-transfer product is formed, most probably accompanied by  $\text{Br}^*$ . The  $\text{I}^- + \text{Br}$  product channel is  $\sim 0.5$  eV lower in energy, and a single  $\text{CO}_2$  solvent molecule does not provide a sufficient solvent electric field to significantly mix those two states. The  $\text{I}^-$ -based products increase to nearly 80% of the total at  $n=4$  and remain relatively constant throughout the range of solvent sizes investigated. Recombined products on the ground state are observed at  $n=7$ , but never become even 10% of the total. For larger cluster sizes, the number of solvent molecules remaining on the product ion can be used to identify the approximate energy of the dissociative asymptote.<sup>34,35</sup> In this case, the number of solvent molecules remaining on  $\text{I}^-$  show that (for  $n \geq 3$ ) the dominant exit channel corresponds to  $\text{I}^- + \text{Br}^*$  dissociation while in the  $a' \ ^2\Pi_{1/2}$  state.

### D. Time-resolved dynamics following excitation of $\text{IBr}^-(\text{CO}_2)_8$ to the $A' \ ^2\Pi_{1/2}$ state

The time-resolved pump-probe studies take advantage of the fact that dissociated  $\text{IBr}^-(\text{CO}_2)_n$  will regain near-IR absorption only after recombination on the ground electronic state. In this experiment, a 790 nm pump pulse excites  $\text{IBr}^-(\text{CO}_2)_8$  to the  $A' \ ^2\Pi_{1/2}$  electronic state. This is the smallest cluster size that affords complete recombination, and, in analogy with the  $\text{I}_2^-(\text{CO}_2)_n$  experiments,<sup>31</sup> absorption recovery was expected to require 10–30 ps.

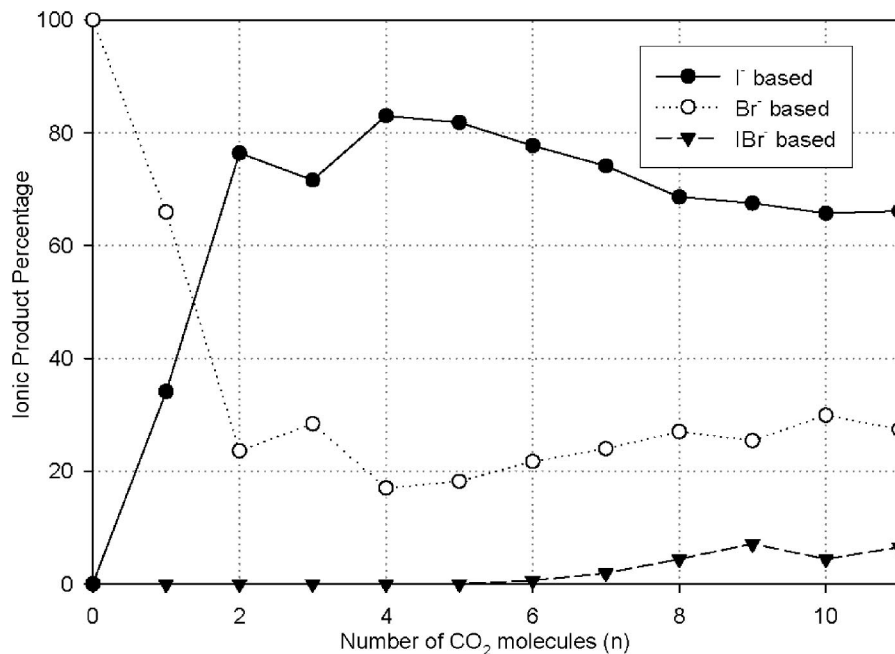


FIG. 7. Photofragmentation products of  $\text{IBr}^-(\text{CO}_2)_n$  cluster ions upon excitation to the  $B$  state with 355 nm photons and an energy release of 1.5 eV in this state.

The pump and the probe wavelengths are both 790 nm with perpendicular polarizations. With appropriate background removal, the measured signal is that portion of the  $\text{I}^-(\text{CO}_2)$  product ion signal that depends upon the presence of both pump and probe pulses. The intensity of this two-photon signal indicates the extent of charge transfer, recombination, and vibrational relaxation on the ground state.

The experimental results for  $\text{IBr}^-(\text{CO}_2)_8$  are shown in Fig. 8. The most striking feature is that there is no detectable recombination signal over the first 200 ps, the maximum delay time available using the precision delay line. The photodissociation measurements reported in Sec. IV B above require that there must be complete absorption recovery within  $\approx 10 \mu\text{s}$ . To find this signal, a crude delay-line arrangement is set up to allow longer delay measurements. The data points at 5 and 8 ns are obtained in this fashion, and a sub-

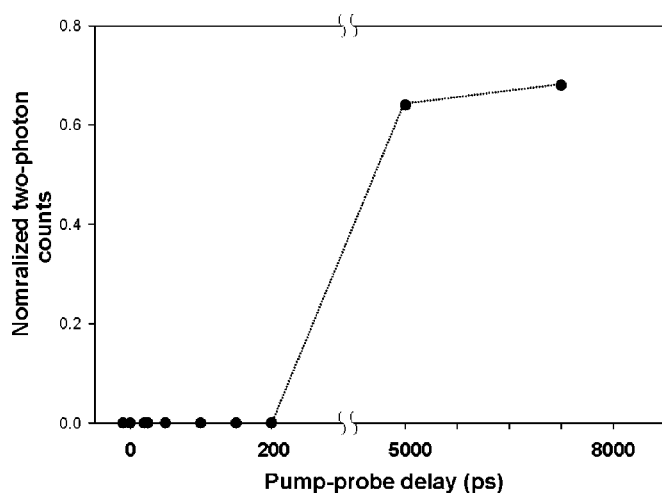


FIG. 8. The  $\text{IBr}^-(\text{CO}_2)_8$  recombination probability as a function of time following excitation to the  $A' \ ^2\Pi$  state with a 790 nm pump pulse. A break is shown to indicate the substantial change in scale. The dashed line is simply to guide the eye.

stantial absorption recovery is now observed! With this crude delay arrangement, the pump-probe pulse overlap is poorly controlled when the delay time is changed, resulting in substantial uncertainty in determining whether the signal is still increasing in this time interval or if it has attained complete absorption recovery. In any event, the  $\gg 200$  ps recombination time scale is striking in comparison with our expectations based on the  $\sim 20$  ps recombination time observed for the smallest  $\text{I}_2^-(\text{CO}_2)_n$  cluster ( $n=12$ ) that shows 100% recombination efficiency for the  $A' \ ^2\Pi_{1/2}$  state.<sup>31</sup>

## V. DISCUSSION

The results presented in Sec. IV document the substantial effects that small numbers of  $\text{CO}_2$  solvent molecules have on the photodissociation dynamics of  $\text{IBr}^-(\text{CO}_2)_n$ . Similar experiments have previously been carried out on  $\text{I}_2^-(\text{CO}_2)_n$  and  $\text{ICl}^-(\text{CO}_2)_n$  cluster ions.<sup>30,31</sup> The results for  $\text{IBr}^-(\text{CO}_2)_n$  are discussed in comparison with the properties of these closely related systems. The comparisons are grouped according to the areas of  $A'$  state excitation,  $B$  state excitation, time-resolved recombination dynamics, charge transfer, and solvent evaporation. In each of these areas, the change from the symmetric  $\text{I}_2^-$  solute to the mixed, asymmetric dihalide has a profound effect on the recombination dynamics.

### A. Dissociation following excitation to the $A' \ ^2\Pi_{1/2}$ state

The solvent dependence of caging  $\text{IBr}^-(\text{CO}_2)_n$  cluster ions following excitation to the  $A' \ ^2\Pi_{1/2}$  state is first compared with that arising from similar excitation in  $\text{ICl}^-(\text{CO}_2)_n$  and  $\text{I}_2^-(\text{CO}_2)_n$  clusters.<sup>30,31</sup> The excitation wavelength for each solute is chosen to provide 0.3 eV energy release in the  $A'$  state. Figure 9 depicts the recombination efficiency as a function of cluster size for these three ions. As is the case for  $\text{ICl}^-$ , the presence of a single  $\text{CO}_2$

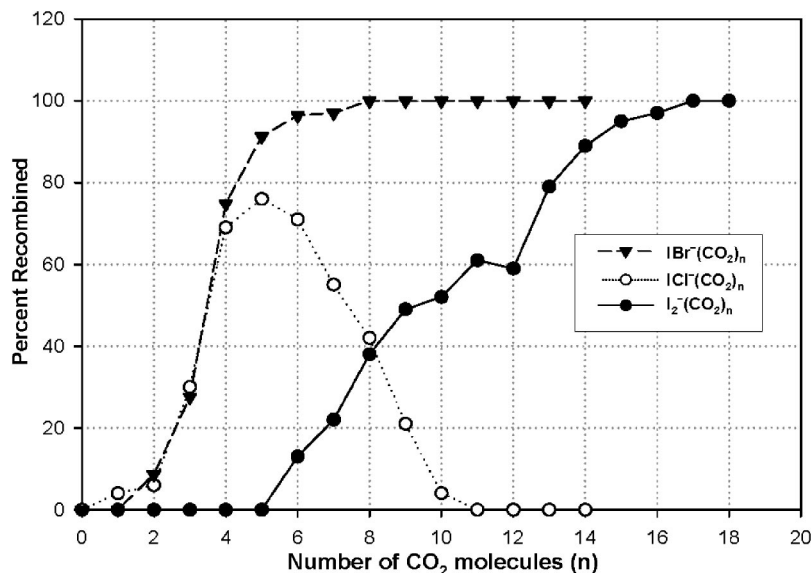


FIG. 9. Recombination percentage for the three solutes as a function of the number of CO<sub>2</sub> molecules upon excitation to the  $A' \ ^2\Pi$  state. The excitation wavelengths are chosen to provide 0.3 eV energy release for each solute.

molecule is sufficient to allow excited  $\text{IBr}^-$  to dissociate on the ground  $^2\Sigma$  state, following charge transfer and a non-adiabatic transition from  $^2\Pi$ . For both  $\text{ICl}^-$  and  $\text{IBr}^-$ , the addition of a second CO<sub>2</sub> solvent molecule both increases the fraction of excited ions reaching the ground state and begins to suppress the ground-state dissociation. Further increases in the number of solvent molecules produce divergent behavior. With increasing solvation,  $\text{IBr}^-(\text{CO}_2)_n$  behaves similarly to  $\text{I}_2^-(\text{CO}_2)_n$ , with both exhibiting increasing recombination percentage with increasing cluster size. However,  $\text{I}_2^-$  recombination first occurs at larger clusters sizes than for  $\text{IBr}^-$  and does not reach 100% recombination until 16 CO<sub>2</sub> molecules have been added, completing the first solvent shell. In contrast,  $\text{IBr}^-(\text{CO}_2)_n$  reaches this limit with only eight CO<sub>2</sub> solvent molecules, which are sufficient to cover only the smaller Br end of the solute (Fig. 4). The same asymmetric solvation appears to retard recombination for  $\text{ICl}^-$ ; as the degree of solvation increases from a half shell to completion of the first solvent shell, the cage fraction decreases from 80% to an undetectable level!

This behavior can be partially rationalized in terms of the properties of the solvent cage depicted for the three dihalide solutes in Fig. 4. To prevent immediate, direct dissociation, at least 0.3 eV must be removed from the dissociating dihalide. The  $\text{IBr}^-(\text{CO}_2)_n$  and  $\text{I}_2^-(\text{CO}_2)_n$  clusters have the first few CO<sub>2</sub> ( $n \leq 4$ ) molecules bind near the waist of the dihalide solutes and only begin to fully enclose one end of the solute (the smaller Br end in the case of  $\text{IBr}^-$ ) with increasing solvation (Fig. 4). For the  $\text{ICl}^-(\text{CO}_2)_n$  clusters, the first CO<sub>2</sub> solvent binds directly to the end of the solute on the much smaller Cl end (not shown) with subsequent solvation continuing around the Cl end (Fig. 4). The efficiency of caging for small  $\text{ICl}^-(\text{CO}_2)_n$  clusters is a result of CO<sub>2</sub> molecules directly in the dissociation pathway for all cluster sizes and the favorable mass match between Cl and CO<sub>2</sub> providing effective energy transfer between the dissociating atom and the solvent. Recombination in  $\text{IBr}^-(\text{CO}_2)_n$  clusters does not occur until  $n=2$  due to the fact that there are no solvent molecules directly in the path of the outgoing disso-

ciated atom at small cluster sizes. However, there are likely cluster structures slightly higher in energy in the experiments that have some solvation directly on the smaller Br end. These structures, coupled with a slightly favorable mass match between Br and CO<sub>2</sub>, lead to recombination at smaller clusters sizes. The  $\text{I}_2^-(\text{CO}_2)_n$  clusters have neither the solvents bound at the end of the solute nor favorable mass match to allow for recombination at small cluster sizes. Recombination does not begin until  $n=6$  for which a substantial cage begins to form around one of the I ends. The observed recombination efficiency in smaller clusters for the three solutes is then highly dependent on the mass match between the dissociated atom and the CO<sub>2</sub> solvent molecules and the position of these solvent molecules at small cluster sizes.

However, the most striking difference between  $\text{I}_2^-(\text{CO}_2)_n$ ,  $\text{IBr}^-(\text{CO}_2)_n$ , and  $\text{ICl}^-(\text{CO}_2)_n$  is the cessation of recombination in  $\text{ICl}^-(\text{CO}_2)_n$  as the solvation increases. Upon excitation to the  $A'$  state in  $\text{ICl}^-(\text{CO}_2)_n$ , there are two deep minima on the potential surface.<sup>42</sup> While the global minimum corresponds to solvated  $\text{ICl}^-$ , there is another deep local minimum corresponding to CO<sub>2</sub> solvated  $\text{Cl}^-$ . This minimum well could easily be accessed during the photodissociation process and deepen with increasing solvation, making it quite possible that this configuration provides the observed trap. The  $\text{IBr}^-$  electronic structure calculations reported here indicate that the  $A' \ ^2\Pi_{1/2}$  state is not purely repulsive, but has a shallow minimum near 3.5 Å. The presence of solvent would deepen this well and could easily prevent the trapping of Br<sup>-</sup>-based products and also account for the very long recombination observed following excitation to the  $A' \ ^2\Pi_{1/2}$  state. Indeed, Sanov<sup>69</sup> has recently seen clear evidence for this minimum in time-resolved photoelectron imaging studies of  $\text{IBr}^-$  excited to the  $A' \ ^2\Pi_{1/2}$  state.

## B. Dissociation following excitation to the $B \ 2^2\Sigma_{1/2}^+$ state

The fraction of the  $\text{I}_2^-(\text{CO}_2)_n$ ,  $\text{ICl}^-(\text{CO}_2)_n$ , and  $\text{IBr}^-(\text{CO}_2)_n$  cluster ions that recombine following excitation

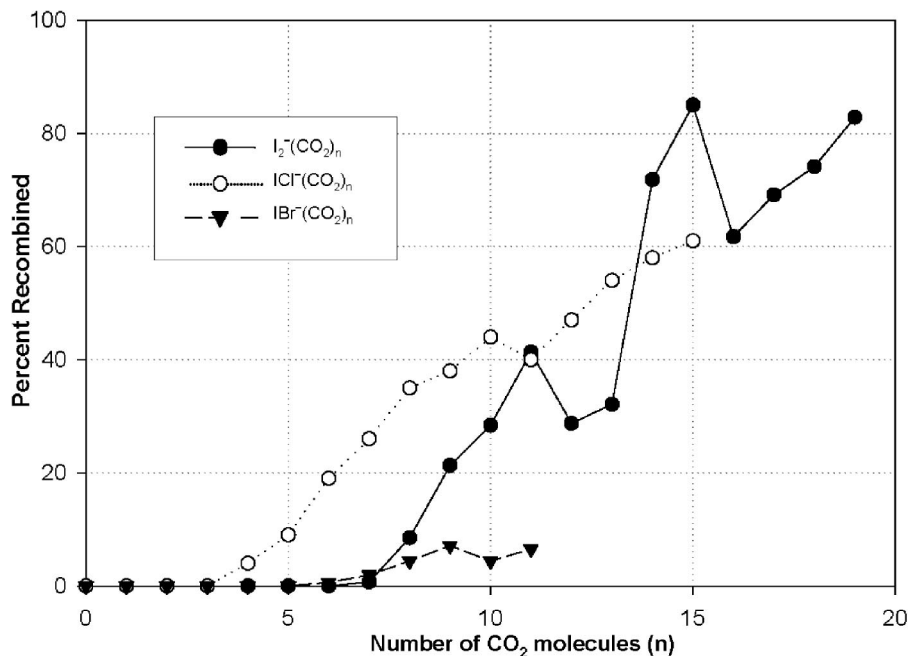


FIG. 10. Recombination percentage for the three solutes as a function of number of  $\text{CO}_2$  molecules, following excitation to the  $B\ 2^2\Sigma$  state. The excitation wavelengths and corresponding energy releases on the  $B$  state are 1.2 eV for  $\text{I}_2^-(\text{CO}_2)_n$ , 0.5 eV for  $\text{ICl}^-(\text{CO}_2)_n$ , and 1.5 eV for  $\text{IBr}^-(\text{CO}_2)_n$ .

to the  $B$  state is shown in Fig. 10. The recombination percentage for  $\text{IBr}^-$  is much less than that of either  $\text{ICl}^-$  or  $\text{I}_2^-$  with similar numbers of solvent molecules. Recombined products first appear at roughly the same cluster size for  $\text{IBr}^-$  and  $\text{I}_2^-$ , with the first  $\text{ICl}^-$  recombination appearing with three fewer  $\text{CO}_2$  solvent molecules. The  $\text{ICl}^-(\text{CO}_2)_n$  clusters now show increasing recombination with increasing cluster size, in contrast to the behavior upon excitation to the  $A'\ 2^2\Pi$  state. Limited molecular dynamics simulations<sup>42</sup> of the recombination of  $\text{ICl}^-$  excited to the  $B\ 2^2\Sigma$  state suggests that the recombination following excitation to this state likely does not access the local minimum preventing recombination following excitation to the  $A'$  state. The  $\text{IBr}^-(\text{CO}_2)_n$  clusters show even less recombination for the largest clusters studied. Much more extensive molecular dynamics simulations will be required to provide a detailed picture of the dynamics involved following the  $B\ 2^2\Sigma$  state excitation.

### C. Time-resolved recombination dynamics

Initial results of the recombination dynamics of  $\text{IBr}^-(\text{CO}_2)_8$  following excitation to the  $A'\ 2^2\Pi_{1/2}$  state show that, while nanoseconds are required for recombination, all of the excited ions survive this process and successfully recombine. This rate is some two orders of magnitude slower than observed for corresponding  $\text{I}_2^-$  clusters that also exhibit complete recombination following  $A'\ 2^2\Pi_{1/2}$  state excitation.<sup>31,70</sup> The discrepancies in absorption recovery times between  $\text{IBr}^-$  and  $\text{I}_2^-$  must be due to the presence of the previously mentioned minimum in the  $\text{IBr}^- A'\ 2^2\Pi_{1/2}$  potential, one that is absent for  $\text{I}_2^-$ . As a consequence of the reduced solvation energy, of  $\text{Br}^-$  compared with  $\text{Cl}^-$ , the atomic anion trap is not as deep for  $\text{Br}^-$ , and apparently the anion can escape, although its escape requires nanoseconds to occur. The long recombination time could also be attributed to a long vibrational relaxation time necessary for ab-

sorption of the probe pulse at lower vibrational levels on the ground state. However, both experiments<sup>37</sup> and simulations<sup>71</sup> performed on  $\text{I}_2^-(\text{CO}_2)_n$  clusters give a vibrational relaxation time once on the ground state of roughly 5 ps. The vibrational frequencies of  $\text{I}_2^-$  and  $\text{IBr}^-$  are not sufficiently different to account for the orders of magnitude difference in the recombination times. Also, previous studies<sup>72</sup> have prepared vibrationally excited  $\text{IBr}^-$  via photodissociation of  $\text{IBr}_2^-$ . The vibrationally excited  $\text{IBr}^-$  is formed in vibrational levels  $\approx 90\%$  of the dissociation energy and exhibit substantial absorption of near-IR wavelengths around 790 nm. For all of these reasons, we conclude that the long absorption recovery time observed for  $\text{IBr}^-(\text{CO}_2)_8$  is a result of excited state dynamics and not a slow vibrational relaxation. This picture, which requires confirmation through extensive simulations, would account for the very slow, but complete recombination of  $\text{IBr}^-(\text{CO}_2)_{n \geq 8}$  excited to the  $A'\ 2^2\Pi_{1/2}$  state.

### D. Solvent evaporation energetics

Analysis of the number of solvent molecules attached to the ionic photoproducts provides important information on the overall recombination energetics, giving both approximate ion-solvent bond energies and providing an accurate identification of the electronic state from which dissociation occurred. We first use the number of solvent molecules remaining on the recombined  $\text{IBr}^-$  ion to determine the average energy removal (solvent binding energy + kinetic energy release) upon evaporation of a single  $\text{CO}_2$  solvent molecule from the ion. This data is then used to identify the electronic state(s) from which dissociation is taking place.

#### 1. Average solvent binding energy

The binding energy of a  $\text{CO}_2$  solvent molecule to the  $\text{IBr}^-$  solute was determined from the average solvent loss found for the recombined products stemming from excitation of  $\text{IBr}^-(\text{CO}_2)_{10-14}$  cluster ions to the  $A'\ 2^2\Pi_{1/2}$  state at three

excitation wavelengths (790, 760, and 675 nm). The photon energy for each wavelength was divided by the average CO<sub>2</sub> solvent loss, yielding the average energy removed by each CO<sub>2</sub> solvent. The three values for the average energy per CO<sub>2</sub> solvent were then themselves averaged to yield an overall average energy removal of 263 ± 12 meV per CO<sub>2</sub> solvent evaporated from IBr<sup>-</sup>. This quantity is very consistent with the average CO<sub>2</sub> energy removal observed<sup>32</sup> for I<sub>2</sub><sup>-</sup>(CO<sub>2</sub>)<sub>*n*</sub> clusters, 250 meV. If the solvent binding energy is desired, then one must estimate the kinetic energy associated with solvent evaporation with a statistical model.<sup>73</sup> This energy release amounts to about 40 meV for IBr<sup>-</sup>(CO<sub>2</sub>), giving an average bond strength of 223 meV for 7–15 CO<sub>2</sub> solvent molecules attached to IBr<sup>-</sup>. For the purpose of identifying the electronic state(s) from which dissociation occurs, this correction adds no uncertainty, as only the average energy removal is required. More detailed solvent evaporation data can be found elsewhere.<sup>74</sup>

## 2. Excitation to the A' 2<sup>2</sup>Π<sub>1/2</sub> state

The first excitation studied is to the A' state in IBr<sup>-</sup>(CO<sub>2</sub>)<sub>*n*</sub> that corresponds to production of I<sup>-</sup> + Br. There is about 0.3 eV energy release on this state corresponding to one CO<sub>2</sub> solvent that would need to be evaporated in the formation of the dissociation products. However, the data show more than one solvent loss for clusters sizes up to *n* = 4, where the I<sup>-</sup> product channel turns off. This result comes from “direct” dissociation of I<sup>-</sup> from the IBr<sup>-</sup> cluster and reflects the inapplicability of a statistical equilibrium model for these very small clusters. For *n* ≥ 13, the average solvent loss has reached a plateau at around six CO<sub>2</sub> solvents lost, exactly what would be expected for nearly complete vibrational relaxation in the ground state. At *n* = 8, the cluster size for which the time-resolved experiments are carried out, there may still be some vibrational excitation in the recombined products, as the ion has lost one fewer than the expected number of CO<sub>2</sub> solvents. This excitation, however, should not shift the photoabsorption spectrum sufficiently to affect the time-resolved measurements.

## 3. Excitation to the B 2<sup>2</sup>Σ<sub>1/2</sub> state

Analysis of the average number of solvent molecules associated with a given ionic photoproduct allows differentiation between the two possible exit channels available for that ionic photoproduct. For example, following excitation of IBr<sup>-</sup>(CO<sub>2</sub>)<sub>11</sub> to the B 2<sup>2</sup>Σ state, a Br<sup>-</sup>-based ion might be associated with either an I atom product (X<sup>2</sup>Σ state dissociation) or an I\* product (B 2<sup>2</sup>Σ state dissociation). With a 250 meV average energy removal per solvent molecule, 355 nm excitation leading to B state dissociation would result in Br<sup>-</sup> production with a concomitant loss of 6–7 solvents, while X state dissociation would result in Br<sup>-</sup> production with a concomitant loss of 10–11 solvent molecules. The observed Br<sup>-</sup> solvent distribution following 355 nm excitation of IBr<sup>-</sup>(CO<sub>2</sub>)<sub>11</sub> peaks at Br<sup>-</sup>(CO<sub>2</sub>)<sub>5</sub>, confirming that this product arises solely from direct dissociation in the initially populated B state. The same conclusion applies to Br<sup>-</sup> products for all of the degrees of solvation investigated here.

The I<sup>-</sup>-based products arising from excitation to the B 2<sup>2</sup>Σ state have a very similar behavior, with the average solvent loss being about one CO<sub>2</sub> fewer than that observed for the corresponding Br<sup>-</sup>-based products. This observation shows that the I<sup>-</sup>-based products arise from dissociation while in the a' 2<sup>2</sup>Π<sub>1/2</sub> state, leading to I<sup>-</sup> and Br\* products. The alternative assignment (A' 2<sup>2</sup>Π state, corresponding to I<sup>-</sup> + Br products) is energetically closer than was the case with Br<sup>-</sup> products, and, while it might be argued that it is close enough to make the assignment ambiguous, such is not the case. Both the sharpness of the product state distribution and the very small recombination fraction observed argue strongly against this alternative assignment.

The dynamics following excitation to the B state for all clusters with more than two CO<sub>2</sub> solvents are determined by the initial curve crossing between the B 2<sup>2</sup>Σ<sub>1/2</sub><sup>+</sup> and a' 2<sup>2</sup>Π<sub>1/2</sub> states. This is very similar to the Marcus-like picture of the dynamics presented for I<sub>2</sub><sup>-</sup>(CO<sub>2</sub>)<sub>*n*</sub> upon excitation to the B state.<sup>57,68</sup> There is an initial step involving either a charge transfer or solvent reorganization around the new charge center. After the branching ratio is determined for this step (either direct dissociation or a charge transfer) at a minimum cluster size, subsequent solvation does not affect this branching ratio.

## VI. SUMMARY

These IBr<sup>-</sup>(CO<sub>2</sub>)<sub>*n*</sub> photodissociation measurements illustrate the richness of phenomena that are observable in size-selected cluster ions. Following the experimental and computational characterization of IBr<sup>-</sup>, photodissociation studies of IBr<sup>-</sup>(CO<sub>2</sub>)<sub>*n*</sub>, *n* < 15, established the central role of the evolving solvent configuration in driving IBr<sup>-</sup> recombination dynamics. Following excitation to the A' 2<sup>2</sup>Π<sub>1/2</sub> state, only recombined products were observed for IBr<sup>-</sup>(CO<sub>2</sub>)<sub>*n*</sub>, *n* ≥ 8. Even though the recombination is complete, the time-resolved recombination dynamics of IBr<sup>-</sup>(CO<sub>2</sub>)<sub>8</sub> exhibited an unexpectedly long (5 ns) time scale for recombination. This result was compared to the <20 ps observed in comparable I<sub>2</sub><sup>-</sup>(CO<sub>2</sub>)<sub>*n*</sub> cluster ions. A shallow well in the A' 2<sup>2</sup>Π<sub>1/2</sub> state appears to trap IBr<sup>-</sup>, leading to long recombination times.

Future experiments will center on extensions of the photodissociation experiments dealing with excitation to the B 2<sup>2</sup>Σ state, as well as additional studies of time-resolved dynamics of not only IBr<sup>-</sup>(CO<sub>2</sub>)<sub>*n*</sub>, but also ICl<sup>-</sup>(CO<sub>2</sub>)<sub>*n*</sub> clusters. The initial pump-probe experiment will be carried out for larger IBr<sup>-</sup>(CO<sub>2</sub>)<sub>*n*</sub> clusters, with probe-pulse delays extended to 5 ns to determine the exact ground state recombination time. A very promising approach for understanding the excited state dynamics in these systems is by time-resolved photoelectron imaging spectroscopy,<sup>75,76</sup> using the velocity map imaging technique of Eppink and Parker.<sup>77</sup> Such experiments are presently in progress in this laboratory. Several experiments have already been carried out that demonstrate the usefulness of this technique on dihalide anions,<sup>69,78</sup> and new details are rapidly emerging about solvation chemistry in this prototypical ionic cluster.

## ACKNOWLEDGMENTS

The authors are pleased to acknowledge support from the National Science Foundation and the Air Force Office of Scientific Research. The authors would also like to acknowledge Dr. Bill Robertson and Professor Mark Johnson for their great help on the pulsed ion source.

- <sup>1</sup>E. Rabinowitch and W. C. Wood, *Trans. Faraday Soc.* **32**, 547 (1936).
- <sup>2</sup>E. Rabinowitch and W. C. Wood, *Trans. Faraday Soc.* **32**, 1381 (1936).
- <sup>3</sup>J. Franck and E. Rabinowitch, *Trans. Faraday Soc.* **30**, 120 (1934).
- <sup>4</sup>A. E. Johnson, N. E. Levinger, and P. F. Barbara, *J. Phys. Chem.* **96**, 7841 (1992).
- <sup>5</sup>D. A. V. Kliner, J. C. Alfano, and P. F. Barbara, *J. Chem. Phys.* **98**, 5375 (1993).
- <sup>6</sup>P. S. Dardi and J. S. Dahler, *J. Chem. Phys.* **93**, 242 (1990).
- <sup>7</sup>D. Booth and R. M. Noyes, *J. Am. Chem. Soc.* **82**, 1868 (1960).
- <sup>8</sup>G. N. R. Tripathi, R. H. Schuler, and R. W. Fessenden, *Chem. Phys. Lett.* **113**, 563 (1985).
- <sup>9</sup>D. J. Nesbitt and J. T. Hynes, *J. Chem. Phys.* **77**, 2130 (1982).
- <sup>10</sup>P. Bado, C. Dupuy, D. Magde, K. R. Wilson, and M. M. Malley, *J. Chem. Phys.* **80**, 5531 (1984).
- <sup>11</sup>A. L. Harris, M. Berg, and C. B. Harris, *J. Chem. Phys.* **84**, 788 (1986).
- <sup>12</sup>N. A. Abul-Haj and D. F. Kelley, *Chem. Phys. Lett.* **119**, 182 (1985).
- <sup>13</sup>Q. Liu, J. K. Wang, and A. H. Zewail, *Nature (London)* **364**, 427 (1993).
- <sup>14</sup>E. D. Potter, Q. Liu, and A. H. Zewail, *Chem. Phys. Lett.* **200**, 605 (1992).
- <sup>15</sup>H. Hippler, K. Luther, and J. Troe, *Chem. Phys. Lett.* **16**, 174 (1972).
- <sup>16</sup>H. Hippler, V. Schubert, and J. Troe, *J. Chem. Phys.* **81**, 3931 (1984).
- <sup>17</sup>K. Luther and J. Troe, *Chem. Phys. Lett.* **24**, 85 (1974).
- <sup>18</sup>K. Luther, J. Schroeder, J. Troe, and U. Unterberg, *J. Phys. Chem.* **84**, 3072 (1980).
- <sup>19</sup>P. B. Beeken, E. A. Hanson, and G. W. Flynn, *J. Chem. Phys.* **78**, 5892 (1983).
- <sup>20</sup>J. G. McCaffrey, H. Kunz, and N. Schwentner, *J. Chem. Phys.* **96**, 2825 (1992).
- <sup>21</sup>H. Kunz, J. G. McCaffrey, R. Schriever, and N. Schwentner, *J. Chem. Phys.* **94**, 1039 (1991).
- <sup>22</sup>R. Zadoyan, Z. Li, P. Ashjian, C. C. Martens, and V. A. Apkarian, *Chem. Phys. Lett.* **218**, 504 (1994).
- <sup>23</sup>R. Zadoyan, Z. Li, C. C. Martens, and V. A. Apkarian, *J. Chem. Phys.* **101**, 6648 (1994).
- <sup>24</sup>A. W. Castleman and K. H. Bowen, *J. Phys. Chem.* **100**, 12911 (1996).
- <sup>25</sup>J. M. Farrar, in *Current Topics in Ion Chemistry and Physics*, edited by C. Y. Ng and I. Powis (Wiley, New York, 1992).
- <sup>26</sup>A. W. Castleman, Jr., in *Clusters of Atoms and Molecules*, edited by H. Haberland (Springer, New York, 1992).
- <sup>27</sup>M. A. Johnson and W. C. Lineberger, in *Techniques for the Study of Ion Molecule Reactions*, edited by J. M. Farrar and J. W. Saunders (Wiley, New York, 1988), p. 591.
- <sup>28</sup>B. J. Greenblatt, M. T. Zanni, and D. M. Neumark, *Chem. Phys. Lett.* **258**, 523 (1996).
- <sup>29</sup>M. T. Zanni, T. R. Taylor, B. J. Greenblatt, B. Soep, and D. M. Neumark, *J. Chem. Phys.* **107**, 7613 (1997).
- <sup>30</sup>M. E. Nadal, P. D. Kleiber, and W. C. Lineberger, *J. Chem. Phys.* **105**, 504 (1996).
- <sup>31</sup>J. M. Papanikolas, V. Vorsa, M. E. Nadal, P. J. Campagnola, H. K. Buchenau, and W. C. Lineberger, *J. Chem. Phys.* **99**, 8733 (1993).
- <sup>32</sup>J. M. Papanikolas, J. R. Gord, N. E. Levinger, D. Ray, V. Vorsa, and W. C. Lineberger, *J. Phys. Chem.* **95**, 8028 (1991).
- <sup>33</sup>V. Vorsa, S. Nandi, P. J. Campagnola, M. Larsson, and W. C. Lineberger, *J. Chem. Phys.* **106**, 1402 (1997).
- <sup>34</sup>S. Nandi, A. Sanov, N. Delaney, J. Faeder, R. Parson, and W. C. Lineberger, *J. Phys. Chem.* **102**, 8827 (1998).
- <sup>35</sup>A. Sanov, T. Sanford, S. Nandi, and W. C. Lineberger, *J. Chem. Phys.* **111**, 664 (1999).
- <sup>36</sup>J. M. Papanikolas, P. J. Campagnola, V. Vorsa, M. E. Nadal, H. K. Buchenau, R. Parson, and W. C. Lineberger, in *The Chemical Dynamics and Kinetics of Small Radicals*, edited by K. Liu and A. Wagner (World Scientific, Singapore, 1995), Vol. 6, p. 616.
- <sup>37</sup>A. V. Davis, R. Wester, A. E. Bragg, and D. M. Neumark, *J. Chem. Phys.* **119**, 2020 (2003).
- <sup>38</sup>A. V. Davis, M. T. Zanni, C. Frischkorn, M. Elhanine, and D. M. Neumark, *J. Electron Spectrosc. Relat. Phenom.* **112**, 221 (2000).
- <sup>39</sup>B. J. Greenblatt, M. T. Zanni, and D. M. Neumark, *Science* **276**, 1675 (1997).
- <sup>40</sup>B. J. Greenblatt, M. T. Zanni, and D. M. Neumark, *J. Chem. Phys.* **112**, 601 (2000).
- <sup>41</sup>J. Faeder, N. Delaney, P. E. Maslen, and R. Parson, *Chem. Phys.* **239**, 525 (1998).
- <sup>42</sup>J. Faeder, Ph.D. thesis, University of Colorado, 1998.
- <sup>43</sup>H. J. Werner, P. J. Knowles, R. Lindh *et al.*, MOLPRO, version 2002.6, a package of *ab initio* programs, see <http://www.molpro.net> (2003).
- <sup>44</sup>H. J. Werner and P. J. Knowles, *J. Chem. Phys.* **89**, 5803 (1988).
- <sup>45</sup>P. J. Knowles and H. J. Werner, *J. Chem. Phys.* **145**, 514 (1988).
- <sup>46</sup>P. J. Knowles and H. J. Werner, *Theor. Chim. Acta* **84**, 95 (1992).
- <sup>47</sup>H. Stoll, B. Metz, and M. Dolg, *J. Comput. Chem.* **23**, 767 (2002).
- <sup>48</sup>H. Stoll (private communication).
- <sup>49</sup>P. E. Maslen, J. Faeder, and R. Parson, *Chem. Phys. Lett.* **263**, 63 (1996).
- <sup>50</sup>P. J. Knowles and H. J. Werner, *Chem. Phys. Lett.* **115**, 259 (1985).
- <sup>51</sup>H. J. Werner and P. J. Knowles, *J. Chem. Phys.* **82**, 5053 (1985).
- <sup>52</sup>A. Berning, M. Schweizer, H. J. Werner, P. J. Knowles, and P. Palmieri, *Mol. Phys.* **98**, 1823 (2000).
- <sup>53</sup>J. Faeder, N. Delaney, P. E. Maslen, and R. Parson, *Chem. Phys. Lett.* **270**, 196 (1997).
- <sup>54</sup>N. Delaney, J. Faeder, P. E. Maslen, and R. Parson, *J. Phys. Chem. A* **101**, 8147 (1997).
- <sup>55</sup>J. Faeder and R. Parson, *J. Chem. Phys.* **108**, 3909 (1998).
- <sup>56</sup>P. E. Maslen, J. Faeder, and R. Parson, *Mol. Phys.* **94**, 693 (1998).
- <sup>57</sup>R. Parson, J. Faeder, and N. Delaney, *J. Phys. Chem. A* **104**, 9653 (2000).
- <sup>58</sup>W. H. Press, S. A. Teukolsky, W. T. Vetterling, and B. P. Flannery, *Numerical Recipes in C: The Art of Scientific Computing*, 2nd ed. (Cambridge University Press, New York, 1992).
- <sup>59</sup>See EPAPS Document No. E-JCPSA6-122-008504 for (1) the minimum energy structures of  $\text{IBr}^-$  with up to 14  $\text{CO}_2$  solvent molecules, as calculated by the method described in the text. A direct link to this document may be found in the online article's HTML reference section. The document may also be reached via the EPAPS homepage (<http://www.aip.org/pubservs/epaps.html>) or from <ftp.aip.org> in the directory `/epaps/`. See the EPAPS homepage for more information.
- <sup>60</sup>W. H. Robertson, J. A. Kelley, and M. A. Johnson, *Rev. Sci. Instrum.* **71**, 4431 (2000).
- <sup>61</sup>V. Vorsa, P. J. Campagnola, S. Nandi, M. Larsson, and W. C. Lineberger, *J. Chem. Phys.* **105**, 2298 (1996).
- <sup>62</sup>N. E. Levinger, D. Ray, M. L. Alexander, and W. C. Lineberger, *J. Chem. Phys.* **89**, 5654 (1988).
- <sup>63</sup>M. Hillenkamp, S. Keinan, and U. Even, *J. Chem. Phys.* **118**, 8699 (2003).
- <sup>64</sup>U. Even, J. Jortner, D. Noy, N. Lavie, and C. Cossart-Magos, *J. Chem. Phys.* **112**, 8068 (2000).
- <sup>65</sup>C. E. Moore, *Atomic Energy Levels* (National Bureau of Standards, Washington, D.C., 1949).
- <sup>66</sup>M. W. Chase, Jr., C. A. Davies, J. R. Downey, Jr., D. J. Frurip, R. A. McDonald, and A. N. Syverud, *J. Phys. Chem. Ref. Data* **14**, 421 (1985), see relevant data on page 421.
- <sup>67</sup>E. Gershgoren and S. Ruhman, private communication.
- <sup>68</sup>N. Delaney, J. Faeder, and R. Parson, *J. Chem. Phys.* **111**, 651 (1999).
- <sup>69</sup>R. Mabbs, K. Pichugin, E. Surber, and A. Sanov, *J. Chem. Phys.* **121**, 265 (2004).
- <sup>70</sup>J. M. Papanikolas, P. E. Maslen, and R. Parson, *J. Chem. Phys.* **102**, 2452 (1995).
- <sup>71</sup>N. Delaney, J. Faeder, and R. Parson, *J. Chem. Phys.* **111**, 452 (1999).
- <sup>72</sup>A. Sanov, T. Sanford, L. J. Butler, J. Vala, R. Kosloff, and W. C. Lineberger, *J. Phys. Chem. A* **103**, 10244 (1999).
- <sup>73</sup>P. C. Engelking, *J. Chem. Phys.* **87**, 936 (1987).
- <sup>74</sup>T. Sanford, Ph.D. thesis, University of Colorado, 2004.
- <sup>75</sup>R. Mabbs, E. Surber, and A. Sanov, *Analyst (Cambridge, U.K.)* **128**, 765 (2003).
- <sup>76</sup>E. Surber, R. Mabbs, and A. Sanov, *J. Phys. Chem. A* **107**, 8215 (2003).
- <sup>77</sup>A. Eppink and D. H. Parker, *Rev. Sci. Instrum.* **68**, 3477 (1997).
- <sup>78</sup>A. V. Davis, R. Wester, A. E. Bragg, and D. M. Neumark, *J. Chem. Phys.* **118**, 999 (2003).